CHEMISTRY

When immiscible becomes miscible—Methane in water at high pressures

Ciprian G. Pruteanu, Graeme J. Ackland, Wilson C. K. Poon, John S. Loveday*

At low pressures, the solubility of gases in liquids is governed by Henry's law, which states that the saturated solubility of a gas in a liquid is proportional to the partial pressure of the gas. As the pressure increases, most gases depart from this ideal behavior in a sublinear fashion, leveling off at pressures in the 1- to 5-kbar (0.1 to 0.5 GPa) range with solubilities of less than 1 mole percent (mol %). This contrasts strikingly with the well-known marked increase in solubility of simple gases in water at high temperature associated with the critical point (647 K and 212 bar). The solubility of the smallest hydrocarbon, the simple gas methane, in water under a range of pressure and temperature is of widespread importance, because it is a paradigmatic hydrophobe and occurs widely in terrestrial and extraterrestrial geology. We report measurements up to 3.5 GPa of the pressure dependence of the solubility of methane in water at 100°C—well below the latter's critical temperature. Our results reveal a marked increase in solubility between 1 and 2 GPa, leading to a state above 2 GPa where the maximum solubility of methane in water exceeds 35 mol %.

INTRODUCTION

Methane is one of the simplest gases, and its solubility in water has been well studied at low pressures. At 100°C, its maximum solubility at 100 bar (10 MPa) is 6×10^{-3} mole percent (mol %), rising to 8×10^{-3} mol % at 2 kbar (*4*). This behavior with an initial linear increase followed by a tendency to level off (*4*) is typical of simple gases (*1*, *2*).

The solution properties of methane in water are important because methane is a model system for studying hydrophobic interaction (*5*). The hydrophobic interaction is of fundamental and wide importance. It is believed to play a crucial role in key biological processes such as protein folding and cell membrane formation (*5*). Hydrophobic interactions are also crucial in the function of detergents and other dispersed systems and hence underlie much of soft-matter science (*5*). In addition, hydrophobic interactions are typical of the dispersion-type forces that underlie much of the behavior of molecular systems in the condensed state. Accurate modeling of such dispersion forces is thus of fundamental importance.

The mixing properties of water-methane are also directly relevant to the green chemistry agenda. Here, one aim is to replace expensive, environmentally hazardous solvents (*6*). Methane is a model for more complex organic systems and an important chemical feedstock in itself.

Finally, methane-water mixtures also occur widely in nature. Methane hydrates are found at the bottom of the oceans, and the outer solar system (notably Uranus, Neptune, and Titan) contains significant proportions of methane and water (*7*, *8*). Knowledge of the speciation of water and methane under planetary conditions is vital for models of planetary interiors. For example, the magnetic fields of Uranus and Neptune are believed to be produced by convection in their icy mantles (*9*). The degree to which methane is soluble in this ice layer strongly affects properties such as density and viscosity, which control convection.

To date, the only information on methane solubility at high pressure has been obtained from simulations. An ab-initio molecular dynamics study beyond 15 GPa and 1800 K found evidence of mixing under these conditions (*10*). However, the temperatures involved were much higher than that of the critical point of water (0.02 GPa and 647 K), where enhanced solubility in water is a well-known phenomenon (*3*). Of more relevance to subcritical water, Hummer *et al.* (*11*) explored the behavior of methane and water up to 0.7 GPa at room temperature using an information theory–based method and classical molecular dynamics. They found that increasing pressure reduced the forces favoring methane aggregation, suggesting a trend toward dispersion of methane and, hence, increased solubility. There are also x-ray diffraction, Raman, and visual observation studies of the methane hydrate decomposition curve up to 600 K and 5 GPa (*12*). These studies provide little information on the decomposed liquid/fluids, but they do report that the hydrate decomposes into two unmixed liquids at an unspecified pressure (*12*). Finally, on the basis of the presumed pressure-induced breaking of the H bonds in water, Chandler (*5*) predicted increased solubility of water in methane, although the magnitude of the effect was unquantified; experimental studies cast doubt on the basis of this prediction, because they show that, instead of breaking the H bonds as had been assumed (*5*), pressure increases the density of water in a way that retains full H bonding up to at least 6.5 GPa (*13*).

RESULTS

Figure 1 shows a sample with 19 mol % methane during a cycle of heating and pressurization. The "as loaded sample" at 1.3 GPa and room temperature is completely solid (Fig. 1A) and is in the form of methane hydrate II and ice VI (note the angular crystals) (*17*). Upon heating, the methane hydrate II decomposed into fluid methane and liquid water at around 330 K to produce a demixed assembly of two distinct fluids (Fig. 1B, note the rounded droplets). Initially, there were numerous small droplets, but over a period of 10 to 20 min at 330 K, these droplets coalesced into larger drops (Fig. 1C). Raman spectroscopy (*18*, *19*) in the region of the methane C–H and water O–H vibrons (~3000 cm^{-1}) showed two fluids with distinct spectra.

Raman spectra collected with the illuminating beam in one fluid (Fig. 1, plot 1) showed a very weak C–H feature at ~2940 cm^{-1} (*20*) and a broad O–H vibron centered at ~3190 cm^{-1} (*21*), indicating that this fluid is methane-poor. Spectra taken from the other fluid (plot 2) showed a much stronger C–H vibron and no evidence of the O–H vibron, suggesting that this fluid is water-poor. Note that the relative weakness of the O–H vibron when compared to the C–H vibron means that its absence does not rule out the presence of some water from this

SUPA, School of Physics Astronomy Centre for Science at Extreme Conditions, The University of Edinburgh, Edinburgh, EH9 3JZ, UK.
*Corresponding author. Email: j.loveday@ed.ac.uk

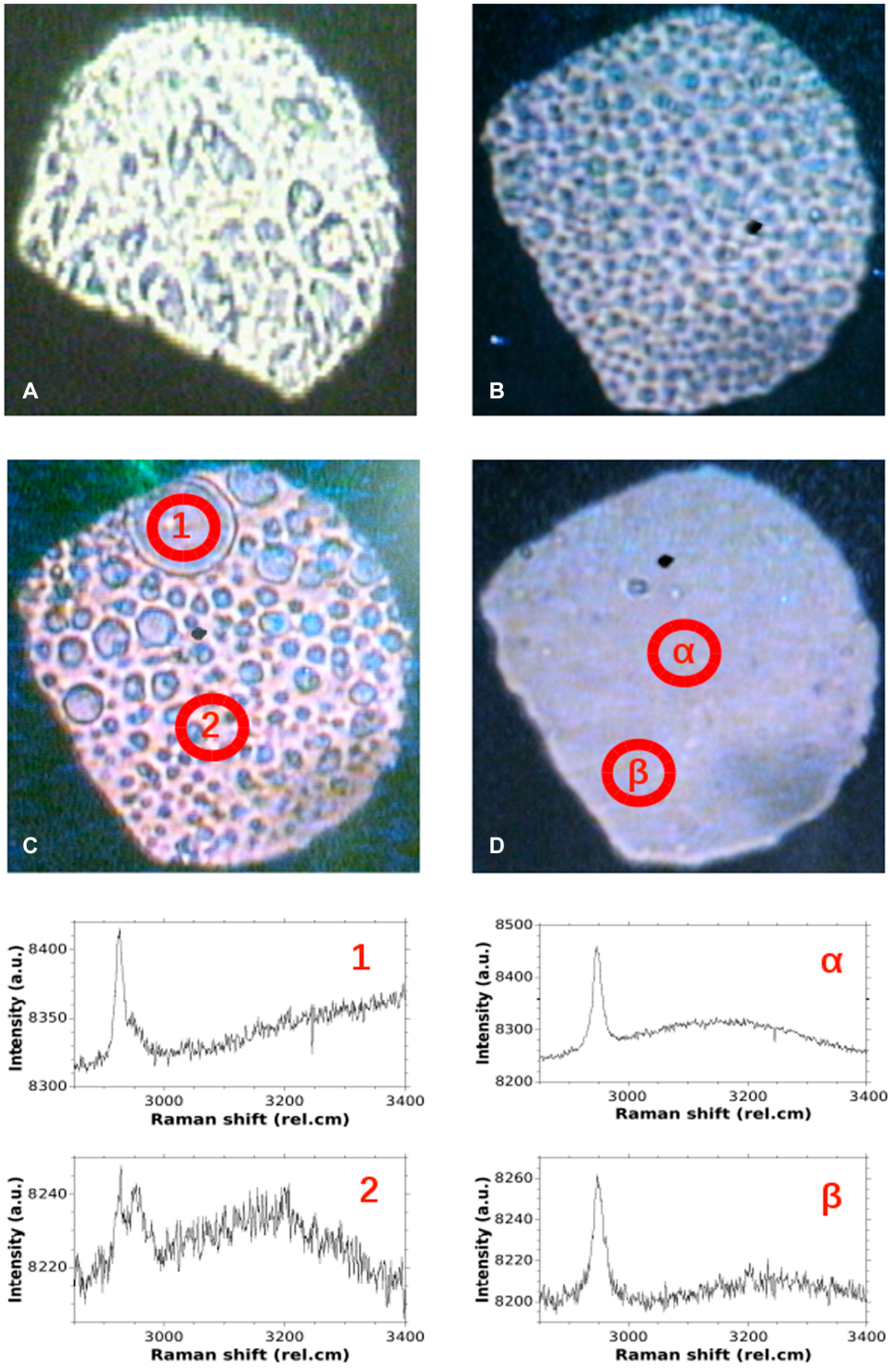

Fig. 1. (**A**) Photomicrograph of a sample of 19 mol % methane water at room temperature and at 1.3 GPa as solid methane hydrate II and ice VI. (**B**) The same sample at 1.3 GPa and 330 K just after decomposition into fluids. (**C**) The sample under the same conditions 0.5 hours later. (**D**) The sample at 330 K and 2 GPa, where it is homogeneous. Plots 1 and 2: Raman spectra taken from positions marked as the open circles labeled 1 and 2, respectively, in (C). In plot 1, the principal peak at ~2850 cm^{-1} is attributed to the C–H stretch mode from methane in the methane-rich fluid. A small secondary peak at ~2900 cm^{-1} is attributed to the C–H stretch from methane dissolved in water (the laser spot whose approximate size is indicated by the circle cannot be entirely confined to the methane-rich region). In plot 2, again the two C–H peaks are visible (because it is not possible to confine the laser spot to the water-rich fluid) along with a broad feature at ~3180 cm^{-1}, which is attributed to the O–H stretch from water. Plots α and β were taken with the laser spot in the positions shown by the open circles labeled α and β, respectively, in (D). Both plots show a single C–H stretch at ~2800 cm^{-1}. Raman spectra were taken at 15 different positions in (D), and all showed the same features as those shown in α and β.

phase. It thus appears that at 1.3 GPa, there is phase separation into coexisting methane-rich and water-rich fluids.

When the pressure was increased to 2 GPa, the area of the methane-rich regions markedly reduced in size and eventually disappeared to give a homogeneous field of view (Fig. 1D). The Raman spectra of this apparently homogeneous liquid showed both O–H and C–H vibrons (plots α and β). Although the intensities varied spatially, no region could be found where the C–H vibron was absent. Increasing the pressure to 2.6 GPa gave no further visual or spectroscopic change.

To explore the composition dependence of the jump in miscibility under pressure, we studied a second sample with 58 mol % methane. This also showed a marked change in visual appearance at 2 GPa (Fig. 2, A and B), with a reduction in the area of the methane-rich liquid. However, above 2 GPa, the sample remained inhomogeneous (B), with a region that showed both C–H and O–H stretch modes and a second region in which only C–H modes were observed. Again, the area of this methane-rich fluid region when compared to that of the rest of the gasket hole was essentially pressure-independent above 2 GPa up to 3.2 GPa at 448 K.

These observations cannot be due to a discontinuous change in the relative compressibilities of methane and water, because there is no such change (*22*, *23*). Neither can our observations be explained by an accidental loss of visual contrast between the two fluids at ~1.9 GPa, because the two fluids remain visible at all pressures in a high-concentration (58 mol %) sample. Much more plausibly, the saturated solubility of methane in water, which is 0 to 5 mol % up to 1.3 GPa, begins to increase at 1.3 GPa, so that the reduction in area of the methane-rich fluid is due to methane dissolving in the water-rich fluid as the pressure is increased. The disappearance of two fluids in the 19 mol % methane sample at 1.9 GPa then implies that above this pressure, the saturated concentration exceeds 19 mol %. The lack of change in the 58% methane sample above 2.0 GPa suggests that above this pressure, the saturated methane concentration is pressure-independent and lies between 19 and 58%. This is an unexpectedly high solubility, given that methane is both hydrophobic and nonpolar.

Assuming that we can approximate the volume fractions of coexisting phases with measured area fractions from micrographs such as those shown in Fig. 1 and making estimates of the excess volume of mixing and the solubility of water in methane at various pressures, it is possible to estimate the concentration of methane in the water-rich fluid using the measured densities (*22*, *23*). Details are given in the online supplementary material. The results plotted in Fig. 3 are robust against wide variations in the estimates we make for the various necessary quantities. The rise in solubility of methane in water starting at around 1.5 GPa is rapid and substantial, taking it from somewhere below 5 mol % (our technique cannot resolve solubilities below 5 mol %) at 1.3 GPa to 41(3) mol % at 2.0 GPa and remaining thereafter.

DISCUSSION

What causes this marked change of the way water dissolves methane at about 1.5 GPa is currently unclear but is unlikely to be a change in the bonding. Structural studies of ice and methane show no marked changes in the inter- or intramolecular bonding in the 1- to 2-GPa range (*24*, *25*). There is a strong change in oxygen coordination in water at these pressures. However, these studies do not show any disruption of the H bond coordination (*13*), as Chandler (*5*) proposed as the basis for the mechanism for increased solubility under pressure. Thus, the mechanism for the pressure-induced solubility we report here differs from the increased solubility of methane observed in supercritical water, which is accompanied by the loss of the H bond network (*26*).

Instead, we suggest that our observations can be explained simply by a continuous reduction in methane molecular size with pressure. Although it is not clear what the relevant size at high pressure is, we do know that the carbon-carbon distance in methane phase 1 is 4.22 Å at ambient pressure, 3.84 Å at 1.6 GPa, and 3.75 Å at 2.9 GPa, values that give an interpolated estimate of 3.81 Å at 2.0 GPa (*27*). By comparison, the H bonds in ice are relatively unchanged by pressure. The ambient pressure H bond distance in ice Ih (2.73 to 2.76 Å) (*28*) is smaller than that in ice VII at 2 GPa (2.93 Å) (*29*). Given these data and the fact that the maximum solubility of methane in water above 2 GPa [41(3) mol %] is close to the methane dihydrate composition (33 mol %), it seems reasonable to speculate that the change in solubility at around 1.5 GPa (Fig. 3) is the result of a change from solvation of the methane in small cage-like structures below 1.3 GPa [as suggested by analogy to crystalline hydrates (*17*, *30*)] to solvation in the channels of an ice I–like H bond network like those of methane dihydrate (methane hydrate phase-III) (*31*). In this hypothesis, the mechanism for this change is simply the continuous compression of the methane diameter combined with the relative lack of compression of the water network, so that at around 1.3 GPa, the methane diameter falls below the critical value needed to allow it to be

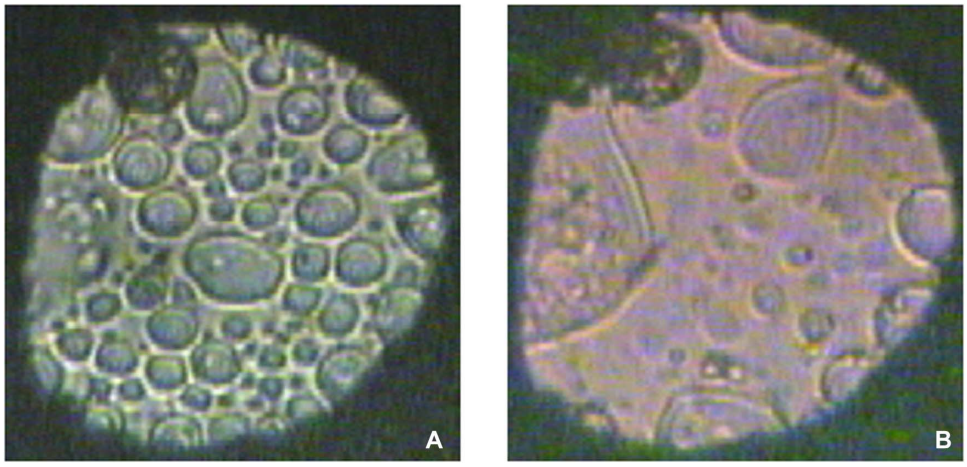

Fig. 2. Photomicrographs of a sample containing 55 mol % methane. (**A**) Shows the sample at 330 K and 1.6 GPa and (**B**) shows it at 330 K and 2.3 GPa. As can be seen, the darker methane-rich regions reduce in area at the higher pressure but the sample remains undifferentiated.

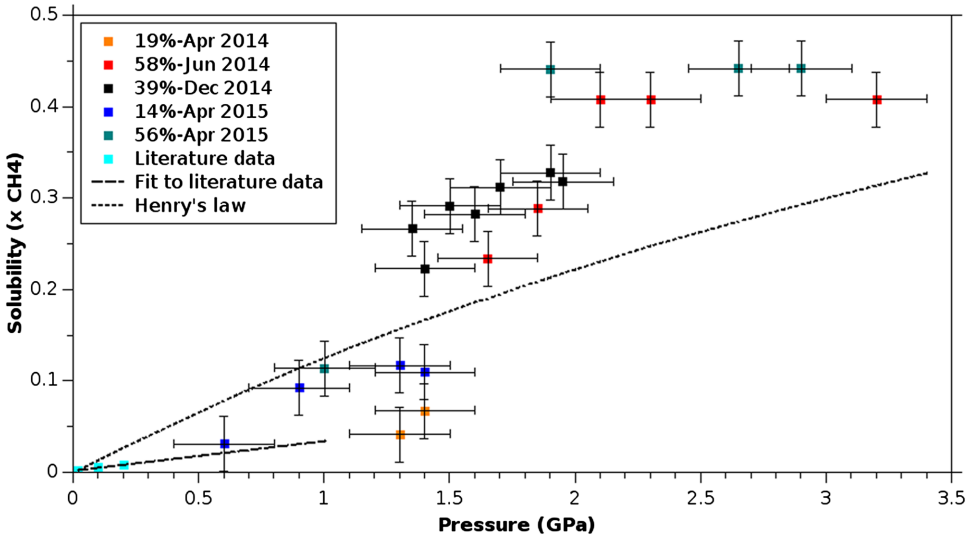

Fig. 3. Plot of the maximum solubility of methane in water at 373 K. The data plotted as points were obtained from the various samples as described in the text. The dotted line shows an extrapolation of Henry's law based on the coefficient determined at ambient pressure (*2*).

dissolved into a fully connected H bond network (*32*). When considered in a bulk thermodynamic way, this process is a balance between the free-energy cost of making cavities in the water network to accommodate the methane and the gains in free energy from the increased entropy of dissolution and the PΔV contribution from producing a mixed phase, which is denser than its unmixed components. Because the cost of making the cavities, the free-energy gain from the entropy of mixing, and the volume change of mixing are all likely to be either pressure-independent or weakly pressure-dependent, it is then almost certain that at some pressure, the increasing magnitude of the PΔV term will make the net free-energy change negative.

If this suggestion is correct, then one might expect to see a similar marked increase in solubility in other clathrate-forming gases, such as nitrogen, oxygen, and the noble gases (*30*), although differences in guest polarizability may also play a role. This concept of a marked change that is produced by a smoothly varying differential compression has been suggested as the origin of the large pressure-induced changes observed in biological systems such as lipid bilayers and proteins (*33*, *34*). The fact that we observe it in a simple system such as methane and water both provides a model system to study such differential effects and highlights the need to understand how the structure of water in biomolecules changes with pressure.

Whatever the mechanism, this step increase in solubility has profound consequences. First, it alters our basic understanding of what solute dissolves in what solvent. In particular, our results show that a property like "hydrophobicity" is not absolute, but can be "tuned" (turned off to some extent) by the application of relatively modest pressures. Second, it is likely that if liquid methane and water occur in the interiors of planetary bodies, then they are never phase-separated.

Finally, our results open up new technological possibilities. They offer routes to new chemical reaction pathways at high pressures. Green chemistry requires new means of functionalizing C–H bonds in water (*6*). The halogenation of methane and the low-temperature catalytic conversion of methane to methanol are foundational and important reactions in this category. Radical increase in the solubility of methane will undoubtedly transform the kinetics of these reactions, if not the mechanism itself. Moreover, if the solubility increase can be brought to occur at a lower pressure than 1 GPa, perhaps by the introduction of a new component to the water network, it may be possible to use such modified water as a novel solvent for green organic chemistry.

Finally, high solubility of gas in water offers a new and potentially very effective way to produce nanobubbles (*35*). Nanobubbles are solutions of small (1- to 100-nm diameter) gas bubbles in water. The arrangement of the H bonds in their surface leads to a surface charge layer, which causes the bubbles to repel each other and hence to avoid agglomeration. Because of their high surface area–to–volume ratio, nanobubbles can enhance the rates of gas solution reactions (*35*). Evidence of nanobubble formation from decomposing clathrate hydrates has already been observed (*36*). Rapid decompression of a high-concentration solution, such as 40% methane/water, into the low solubility pressure range may prove an effective means to nucleate very high concentrations of nanobubbles.

MATERIALS AND METHODS

We loaded samples of distilled water and methane into Merrill-Bassett–type diamond anvil cells using steel gaskets (*14*). The composition of the sample was controlled as follows. First, the gasket hole was completely filled with water. The cell was observed as the water evaporated and an air bubble formed. Once the bubble was of a suitable size, the cell was lightly sealed to prevent further evaporation and placed in a pot, which was cooled to ~100 K. Methane was condensed into the pot covering the cell, which was opened to allow the methane to fill the bubble in the now frozen water. After sealing, the cell was allowed to warm to room temperature. The pressure was adjusted to 1 to 1.5 GPa (determined by ruby fluorescence) and left to equilibrate overnight. The composition of the sample was estimated from measurements of the relative areas of the bubble and that part of the gasket filled with water using a microscope. Assuming that the bubble and the water-filled region had the same thickness, we calculated the proportions of methane and water from the densities of methane (*15*) and ice at 100 K (*16*). This procedure is described in the online material and is accurate to 3 to 5 mol %. For the experiments, the cell was mounted on a combined micro-Raman and direct observation system. The sample was illuminated by white light from behind and observed using a digital camera. The exciting laser

for the Raman was a diode laser with a wavelength of 532 nm. The cell was heated externally using a resistive heater, and the temperature was measured by a thermocouple touching the back of the diamonds. Before each experiment, the Raman system was calibrated using the emission lines from a neon lamp.

REFERENCES AND NOTES

1. P. W. Atkins, P. J. De, *Atkins' Physical Chemistry* (Oxford Univ. Press, 2010).
2. R. Sander, Compilation of Henry's law constants (version 4.0) for water as solvent. *Atmos. Chem. Phys.* **15**, 4399–4981 (2015).
3. K. Yamanaka, H. Ohtaki, *Thermodynamics, Solubility and Environmental Issues*, T. M. Letcher, Ed. (Elsevier, 2007), pp. 51–79.
4. Z. Duan, S. Mao, A thermodynamic model for calculating methane solubility, density and gas phase composition of methane-bearing aqueous fluids from 273 to 523 K and from 1 to 2000 bar. *Geochim. Cosmochim. Acta* **70**, 3369–3386 (2006).
5. D. Chandler, Interfaces and the driving force of hydrophobic assembly. *Nature* **437**, 640–647 (2005).
6. C. I. Herrerías, X. Yao, Z. Li, C. J. Li, Reactions of C-H bonds in water. *Chem. Rev.* **107**, 2546–2562 (2007).
7. J. I. Lunine, D. J. Stevenson, Clathrate and ammonia hydrates at high pressure: Application to the origin of methane on Titan. *Icarus* **70**, 61–77 (1987).
8. T. Guillot, The interiors of giant planets: Models and outstanding questions. *Annu. Rev. Earth Planet. Sci.* **33**, 493–530 (2005).
9. S. Stanley, J. Bloxham, Convective-region geometry as the cause of Uranus' and Neptune's unusual magnetic fields. *Nature* **42**, 151–153 (2004).
10. M.-S. Lee, S. Scandolo, Mixtures of planetary ices at extreme conditions. *Nat. Commun.* **2**, 185 (2011).
11. G. Hummer, S. Garde, A. E. García, M. E. Paulaitis, L. R. Pratt, The pressure dependence of hydrophobic interactions is consistent with the observed pressure denaturation of proteins. *Proc. Natl. Acad. Sci. U.S.A.* **95**, 1552–1555 (1998).
12. L. Bezacier, E. Le Menn, O. Grasset, O. Bollengier, A. Oancea, M. Mezouar, G. Tobie, Experimental investigation of methane hydrates dissociation up to 5 GPa: Implications for Titan's interior. *Phys. Earth Planet. In.* **22**, 144–152 (2014).
13. T. Strässle, A. M. Saitta, Y. Le Godec, G. Hamel, S. Klotz, J. S. Loveday, R. J. Nelmes, Structure of dense liquid water by neutron scattering to 6.5 GPa and 670 K. *Phys. Rev. Lett.* **96**, 067801 (2006).
14. L. Merrill, W. A. Bassett, Miniature diamond anvil pressure cell for single crystal x-ray diffraction studies. *Rev. Sci. Instrum.* **45**, 290–294 (1974).
15. U. Setzmann, W. Wagner, A new equation of state and tables of thermodynamic properties for methane covering the range from the melting line to 625 K at pressures up to 1000 MPa. **20**, 1061–1155 (1991).
16. A. G. Ogienko, A. V. Kurnosov, A. Y. Manakov, E. G. Larionov, A. I. Ancharov, M. A. Sheromov, A. N. Nesterov, Gas hydrates of argon and methane synthesized at high pressures: Composition, thermal expansion, and self-preservation. *J. Phys. Chem. B* **110**, 2840–2846 (2006).
17. J. S. Loveday, R. J. Nelmes, M. Guthrie, S. A. Belmonte, D. R. Allan, D. D. Klug, J. S. Tse, Y. P. Handa, Stable methane hydrate above 2 GPa and the source of Titan's atmospheric methane. *Nature* **410**, 661–663 (2001).
18. R. T. Howie, C. L. Guillaume, T. Scheler, A. F. Goncharov, E. Gregoryanz, Mixed molecular and atomic phase of dense hydrogen. *Phys. Rev. Lett.* **108**, 125501 (2012).
19. P. Dalladay-Simpson, R. T. Howie, E. Gregoryanz, Evidence for a new phase of dense hydrogen above 325 gigapascals. *Nature* **529**, 63–67 (2016).
20. H. Shimizu, T. Kumazaki, T. Kume, S. Sasaki, In situ observations of high-pressure phase transformations in a synthetic methane hydrate. *J. Phys. Chem. B* **106**, 30–33 (2002).
21. Y. Ohno, S. Sasaki, T. Kume, H. Shimizu, High-pressure raman study on single crystalline methane hydrate surrounded by methane in a diamond anvil cell. *J. Phys. Conf. Ser.* **121**, 42014 (2008).
22. M. Li, F. Li, W. Gao, C. Ma, L. Huang, Q. Zhou, Q. Cui, Brillouin scattering study of liquid methane under high pressures and high temperatures. *J. Chem. Phys.* **133**, 044503 (2010).
23. E. H. Abramson, J. M. Brown, Equation of state of water based on speeds of sound measured in the diamond-anvil cell. *Geochim. Cosmochim. Acta* **68**, 1827–1835 (2004).
24. R. J. Nelmes, J. S. Loveday, R. M. Wilson, J. M. Besson, P. Pruzan, S. Klotz, G. Hamel, S. Hull, Neutron diffraction study of the structure of deuterated ice VIII to 10 GPa. *Phys. Rev. Lett.* **71**, 1192–1195 (1993).
25. H. E. Maynard-Casely, C. L. Bull, M. Guthrie, I. Loa, M. I. McMahon, E. Gregoryanz, R. J. Nelmes, J. S. Loveday, The distorted close-packed crystal structure of methane A. *J. Chem. Phys.* **133**, 064504 (2010).
26. P. Postorino, R. H. Tromp, M.-A. Ricci, A. K. Soper, G. W. Neilson, The interatomic structure of water at supercritical temperatures. *Nature* **366**, 668–670 (1993).
27. R. M. Hazen, H. K. Mao, L. W. Finger, P. M. Bell, Structure and compression of crystalline methane at high pressure and room temperature. *Appl. Phys. Lett.* **37**, 288–289 (1980).
28. A. J. Leadbetter, R. C. Ward, J. W. Clark, P. A. Tucker, T. Matsuo, H. Suga, The equilibrium low-temperature structure of ice. *J. Chem. Phys.* **82**, 424–428 (1985).
29. W. F. Kuhs, J. L. Finney, C. Vettier, D. V. Bliss, Structure and hydrogen ordering in ices VI, VII, and VIII by neutron powder diffraction. *J. Chem. Phys.* **81**, 3612–3623 (1984).
30. J. S. Loveday, R. J. Nelmes, High-pressure gas hydrates. *Phys. Chem. Chem. Phys.* **10**, 937–950 (2008).
31. J. S. Loveday, R. J. Nelmes, M. Guthrie, D. D. Klug, J. S. Tse, Transition from cage clathrate to filled ice: The structure of methane hydrate III. *Phys. Rev. Lett.* **87**, 215501 (2001).
32. P. Buchanan, A. K. Soper, H. Thompson, R. E. Westacott, J. L. Creek, G. Hobson, C. A. Koh, Search for memory effects in methane hydrate: Structure of water before hydrate formation and after hydrate decomposition. *J. Chem. Phys.* **123**, 164507 (2005).
33. B. Barstow, N. Ando, C. U. Kim, S. M. Gruner, Alteration of citrine structure by hydrostatic pressure explains the accompanying spectral shift. *Proc. Natl. Acad. Sci. U.S.A.* **105**, 13362–13366 (2008).
34. P. T. C. So, S. Gruner, S. Erramilli, Pressure-induced topological phase-transitions in membranes. *Phys. Rev. Lett.* **70**, 3455–3458 (1993).
35. M. Alheshibri, J. Qian, M. Jehannin, V. S. J. Craig, A history of nanobubbles. *Langmuir* **32**, 11086–11100 (2016).
36. L. Yang, A. Falenty, M. Chaouachi, D. Haberthür, W. F. Kuhs, Synchrotron x-ray computed microtomography study on gas hydrate decomposition in a sedimentary matrix. *Geochem. Geophys. Geosyst.* **17**, 3717–3732 (2016).

Acknowledgments: We would like to acknowledge E. Gregoryanz, R. Howie, and M.-E. Donnelly for help with the experiments and P. McMillan for the helpful discussions. **Funding:** This work was supported by the Engineering and Physical Sciences Research Council (EPSRC) through a Centre for Doctoral Training studentship for C.G.P. and through a Royal Society Wolfson Fellowship and an ERC advanced grant HECATE for G.J.A. **Author contributions:** J.S.L. conceived the experiment, directed the work, and wrote the first draft of the manuscript. C.G.P. performed the experiment and the data analysis and participated in the preparation of the manuscript. W.C.K.P. helped to direct the work, participated in the data interpretation, and substantially redrafted the manuscript. G.J.A. contributed insights on the possible mechanism of the change in solubility. **Competing interests:** The authors declare that they have no competing interests. **Data and materials availability:** All data needed to evaluate the conclusions in the paper are present in the paper. Raw data will be made available online through the University of Edinburgh Data repository http://datashare.is.ed.ac.uk/handle/10283/2771.

Submitted 23 January 2017
Accepted 26 July 2017
Published 23 August 2017
10.1126/sciadv.1700240

Citation: C. G. Pruteanu, G. J. Ackland, W. C. K. Poon, J. S. Loveday, When immiscible becomes miscible—Methane in water at high pressures. *Sci. Adv.* **3**, e1700240 (2017).